

Low voltage performance of epitaxial BiFeO₃ films on Si substrates through lanthanum substitution

Y. H. Chu, Q. Zhan, C.-H. Yang, M. P. Cruz, L. W. Martin et al.

Citation: *Appl. Phys. Lett.* **92**, 102909 (2008); doi: 10.1063/1.2897304

View online: <http://dx.doi.org/10.1063/1.2897304>

View Table of Contents: <http://apl.aip.org/resource/1/APPLAB/v92/i10>

Published by the [American Institute of Physics](http://www.aip.org).

Additional information on *Appl. Phys. Lett.*

Journal Homepage: <http://apl.aip.org/>

Journal Information: http://apl.aip.org/about/about_the_journal

Top downloads: http://apl.aip.org/features/most_downloaded

Information for Authors: <http://apl.aip.org/authors>

ADVERTISEMENT



Goodfellow
metals • ceramics • polymers • composites
70,000 products
450 different materials
small quantities fast

www.goodfellowusa.com

Low voltage performance of epitaxial BiFeO₃ films on Si substrates through lanthanum substitution

Y. H. Chu,^{1,a)} Q. Zhan,¹ C.-H. Yang,¹ M. P. Cruz,¹ L. W. Martin,¹ T. Zhao,¹ P. Yu,¹ R. Ramesh,¹ P. T. Joseph,² I. N. Lin,² W. Tian,³ and D. G. Schlom³

¹Department of Materials Science and Engineering and Department of Physics, University of California, Berkeley, California 94720, USA

²Department of Physics, Tamkang University, Tamsui, Taiwan 251, Republic of China

³Department of Materials Science and Engineering, Pennsylvania State University, University Park, Pennsylvania 16802, USA

(Received 8 January 2008; accepted 21 February 2008; published online 14 March 2008)

We have probed the role of La substitution on the ferroelectric properties of epitaxial BiFeO₃ films on SrTiO₃-templated Si. This provides a mechanism to engineer the rhombohedral distortion in the crystal and, thus, control domain structure and switching. With a 10% La substitution, the (Bi_{0.9}La_{0.1})FeO₃ film showed well-saturated ferroelectric hysteresis loops with a remanent polarization of 45 μC/cm², a converse piezoelectric coefficient *d*₃₃ of 45 pm/V, and a dielectric constant of 140. Over this range of La substitution, the coercive field systematically decreases such that a coercive voltage of 1 V can be obtained in a 100 nm thick film. These results show promise for the ultimate implementation of this lead-free multiferroic operating at voltages in the range of 2–3 V. © 2008 American Institute of Physics. [DOI: 10.1063/1.2897304]

Room temperature (RT) single phase multiferroics, materials which simultaneously show a spontaneous magnetization and polarization, remain elusive as most such multiferroic systems exhibit the coexistence of multiple order parameters only at low temperatures.^{1,2} BiFeO₃ (BFO) is a RT multiferroic (ferroelectric and antiferromagnetic). Epitaxial thin films of this material have been shown to exhibit large polarizations making it a candidate “green” ferro/piezoelectric material to replace the cornerstone lead zirconate titanate (PZT) family. Our previous results also showed a model approach to integrate BFO films on Si substrates by using an SrTiO₃ (STO) template layer with an SrRuO₃ (SRO) bottom electrode.^{3,4} However, we also noted that these films on Si show a coercive field of 200 kV/cm and a large leakage level, which are obstacles to actual device applications. Lowering the coercive field to a value below 100 kV/cm as well as the leakage have, thus, become critical issues. In this paper, we demonstrate through a systematic series of experiments that La substitution at the Bi site enables such a control over the coercive field (although it does not impact the leakage properties significantly, all samples show the leakage about 10⁻⁴ A/cm² at 2 V).

In bulk, it has been reported that rare-earth ions can be substituted for the Bi³⁺ cation in BFO.⁵ Such an isovalent substitution is not expected to change the defect chemistry of these perovskites, unlike in the case of the PZT system. However, substituting Bi with La is expected to change both the Curie temperature and the lattice constant.^{6,7} This could then provide a mechanism by which one could “tune” the rhombohedral distortion in the crystal and, thus, control both the switching mechanism and therefore the coercive field. The structural and ferroelectric properties of the (Bi_{1-x}La_x)FeO₃ (LBFO) thin films which correlate with different La concentrations and thickness are discussed.

Epitaxial LBFO (0%, 10%, 15%, and 20% La substitution) films were synthesized by pulsed laser deposition on single crystal STO(001)/Si(001) substrates.⁸ Epitaxially grown SRO was used as top and bottom electrodes because of its good lattice match with both BFO and STO.⁹ The crystallinity of the (L)BFO films were studied by x-ray diffraction (XRD) (Panalytical X’Pert MRD Pro) and transmission electron microscopy (TEM) (JEOL 3010 operating at 300 kV). The typical XRD θ - 2θ scans shown in Fig. 1(a) reveal the crystallinity and crystallographic orientation of the (L)BFO films. The 0%, 10%, and 15% LBFO films exhibit the perovskite structure and are likely to possess rhombohedral symmetry. The out-of-plane lattice parameters of all these films are ~3.95 Å (pseudocubic unit), which is smaller than their bulk values. This can be ascribed to the presence of the in-plane tensile stress induced by the thermal mismatch between Si and the oxide film. In contrast, for the 20% LBFO film, each (00*l*) line is split into two peaks corresponding to out-of-plane lattice parameters of 3.90 and 3.95 Å. Detailed selected area electron diffraction analyses,

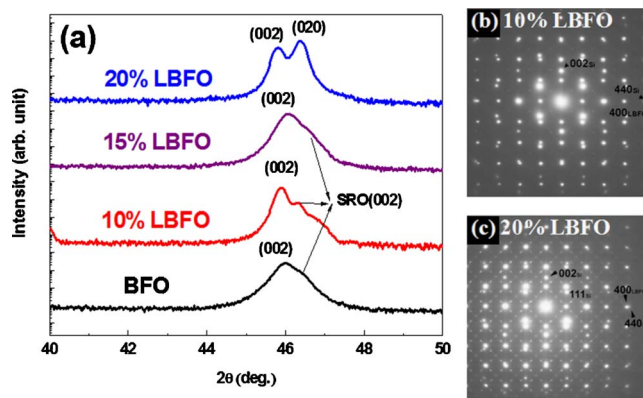


FIG. 1. (Color online) (a) Typical x-ray θ - 2θ scans of the BFO and LBFO films with different La concentrations on SRO/STO/Si substrates. Electron diffraction patterns of (b) 10% and (c) 20% LBFO films.

^{a)}Electronic mail: yhchu@lbl.gov.

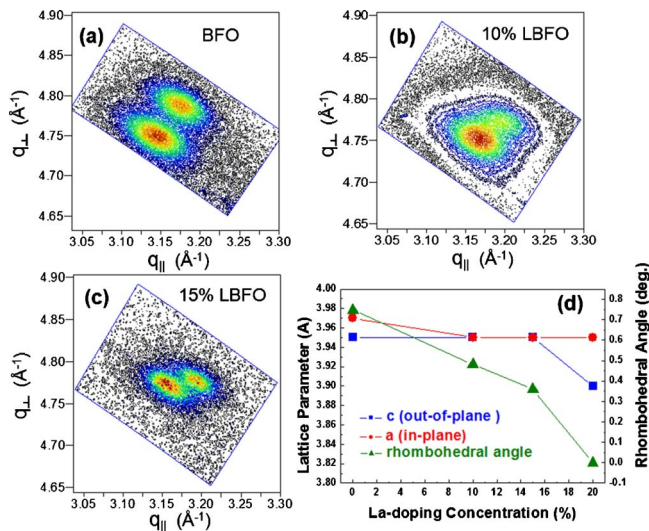


FIG. 2. (Color online) Reciprocal space maps (RSMs) represented in reciprocal-lattice units for (a) BFO, (b) 10% LBFO, and (c) 15% LBFO films. (d) The summary of the lattice parameters and rhombohedral angles.

[Figs. 1(b) and 1(c)] reveal a change to an orthorhombic structure at a 20% La concentration, consistent with bulk data.¹⁰ The two peaks correspond to the two structural domains (*c* and *b* domains) of the orthorhombic phase.

To fully understand the structural evolution of the (L)BFO films, XRD reciprocal space mapping (RSM) was employed. The 203_{pc} (where *pc* refers to the pseudocubic structure of BFO) diffraction peak was selected because it possesses in-plane directional information necessary to give us a signature of the true crystal symmetry. Figures 2(a)–2(c) show RSMs for (L)BFO films of varying La concentration. For all the rhombohedral samples, we observed clear splitting of the 203_{pc} BFO peaks. Both upward and downward peaks can be detected simultaneously on the single RSM, owing to the four-variant twinlike domain structure.¹¹ The splitting between the two peaks yields the rhombohedral angle and distortion direction along the [110]. The summary of lattice parameters and rhombohedral angles for (L)BFO is shown in Fig. 2(d). It clearly shows for rhombohedral (L)BFO films the lattice parameters remain close to bulk value, however, the rhombohedral angles decrease as the La

concentration is increased (from 0.75° for BFO to 0.36° for 15% LBFO).

Since the crystal structure has been modified, the next step is to explore the corresponding electrical properties. Pt/SRO top electrodes ($32 \mu\text{m}$ in diameter) were patterned by ion beam etching in order to measure the ferroelectric properties with a RT-6000 ferroelectric testing station. The capacitance-voltage (*C-V*) behavior was measured by an impedance analyzer (HP 4194A). Morphology and local piezoelectric properties were investigated using an atomic force microscope-based setup. The capacitor structure after processing is revealed in a cross-sectional TEM image [Fig. 3(a)], showing a clear, smooth interface between SRO and (L)BFO. Energy dispersive spectroscopy (EDS) was also performed *in situ* with the TEM analysis, and indicates that there is no interdiffusion at either the top or bottom interface which makes such a device structure promising for electrical measurements. The macroscopic electrical polarization-field (*P-E*) hysteresis loops, measured by a hysteresis loop tracer at 20 kHz, of the (L)BFO films are shown in Fig. 3(b). Only the rhombohedrally structured films show sharp, square loops and yield a $2P_r$ value of $80\text{--}90 \mu\text{C}/\text{cm}^2$. Most importantly, a significant reduction of the coercive field from 200 kV/cm for the BFO film to 90 kV/cm was observed in the 15% LBFO film. The 20% LBFO films show no *P-E* hysteresis, as a consequence of the structural change to the nonferroelectric, orthorhombic phase.¹² The electric field dependence of the dielectric constant $\epsilon_r(E)$ was measured by a capacitance-voltage (*C-V*) tester at 1 MHz (not shown). The observed butterfly-type hysteresis loops in the ϵ_r -*E* measurements are characteristic of polarization switching. The zero-field small-signal ϵ_r is around ~ 100 for the BFO films, ~ 140 for the 10%-LBFO films, and ~ 185 for the 15%-LBFO films, indicating that the dielectric response of the films increases due to La addition. This result is in agreement with the previously reported data in bulk materials¹² and polycrystalline films.¹³ The capacitance peaks occur at a field value corresponding to the films' coercive fields (E_C), that is about 160 kV/cm for BFO and 80 kV/cm for the LBFO films, indicating again that the latter exhibit a smaller coercivity. Quantitative out-of-plane piezoelectric response measurements (not shown), showed that the coercive field of

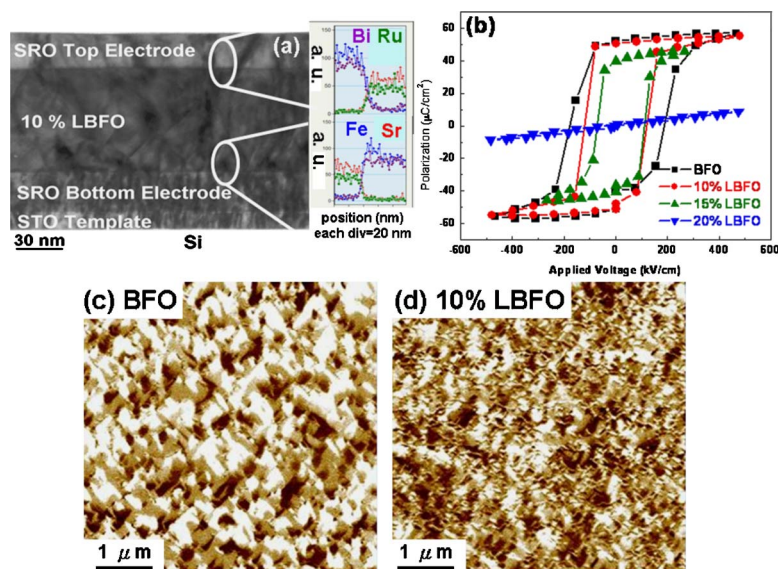


FIG. 3. (Color online) (a) Cross-sectional TEM image and energy dispersive spectroscopy of SRO/LBFO/SRO/STO/Si films. (b) *P-E* hysteresis loops, of BFO and LBFO films with different La concentrations. As grown ferroelectric domain structures of (c) BFO and (d) 10% LBFO films.

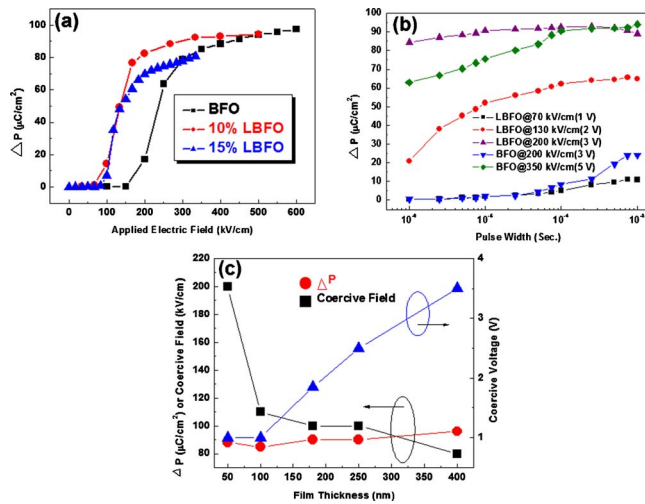


FIG. 4. (Color online) Switched polarization (ΔP) as a function of (a) applied electric field and (b) pulse width. (c) Thickness dependence of the ferroelectric properties (ΔP , coercive field and voltage).

the LBFO film (90 kV/cm) is much smaller than the coercive field of the BFO films (150 kV/cm). A remanent d_{33} of 45 pm/V for the fully clamped 10% LBFO film was observed.

The obvious question is this: why does this substitution of Bi by La lead to a lowering of the coercive field? In order to answer this, piezoelectric force microscopy was also used to study the corresponding domain structures as a function of La content. The as-grown domain structures of BFO and 10% LBFO films are shown in Figs. 3(c) and 3(d), respectively. Clearly three different tones, namely, white, black, and brown, can be found in these images. These three tones for the in-plane PFM images are typical for BFO films measured along $\langle 110 \rangle$.¹¹ The domain size (~ 50 nm) in LBFO films is much smaller than that in BFO (~ 100 nm) films. This significant difference in domain structure is the most important consequence of the lattice engineering approach that La substitution enables, which is key factor to lower the coercivity. Based on phase field simulation and piezoresponse force spectroscopy, Kalinin *et al.*¹⁴ pointed out the domain wall can be a possible scenario for low nucleation voltage in BFO films. As the domain size is much smaller in LBFO, which implies the domain wall density is also much higher, leading to a lower coercive field.

We observed significant differences in the dynamic switching behavior between the BFO and LBFO films. Pulsed polarization measurements yield the switched polarization, $\Delta P = P^* - P^{\wedge}$ (switched polarization) $- P^{\wedge}$ (nonswitched polarization) as a function of applied field as well as pulse width. Figure 4(a) shows the switching polarization (ΔP) as a function of the electric field. The ΔP of the BFO film starts to increase at about 200 kV/cm and saturates at ~ 400 kV/cm , whereas the ΔP for the 10%- and 15%-LBFO films starts to rise at 100 kV/cm and saturates at 300 kV/cm , consistent with the reduction in coercivity for the LBFO films. The saturated switched polarization (ΔP) is consistent with the $2P_r$ value measured with the P - E hysteresis loop tracer. Another important consequence of the lower coercive voltage is that the switched polarization is not sig-

nificantly influenced by the write and read pulse width. We have measured the switched polarization as a function of pulse width for the BFO and LBFO films of 150 nm thickness, the results of which are shown in Fig. 4(b). As the pulse width is decreased from 1 ms to 1 μs , the switched polarization of 10% LBFO remained relatively unchanged at 85 $\mu\text{C}/\text{cm}^2$ at 3 V. It is noteworthy that the LBFO film shows a significant switched polarization (although not the full saturated value) even at a write/read voltage of 2 V and a pulse width of 1 μsec . In stark contrast, the BFO films of the same thickness show a much more sluggish switching behavior. At 3 V, there is hardly any switched polarization at 1 μsec ; even at 5 V there is a strong pulse width dependence of the switched polarization. Operability of the ferroelectric capacitors at low voltage levels is mandatory in future devices. Therefore, we have also studied the thickness-dependent ferroelectric properties of the epitaxial 10% LBFO films on Si. Figure 4(c) contains the summary of these results. The change in ΔP and the coercive field is relatively small. A 100 nm thick film showed a 85 $\mu\text{C}/\text{cm}^2$ switchable polarization which saturated at 2.5 V with a 1.0 V coercive voltage.

In summary, by using an STO template layer and an SRO conducting oxide electrode, epitaxial LBFO films were grown on Si(001) substrates. With La doping, the rhombohedral angle has been modified. As a consequence, the ferroelectric coercive voltage of the BFO films was reduced to a level of 1.0 V by a 10% La substitution of Bi.

The authors acknowledge support of the National Center for Electron Microscopy, Lawrence Berkeley Laboratory, which is supported by the U.S. Department of Energy under Contract No. DE-AC02-05CH11231.

¹N. Hur, S. Park, P. A. Sharma, J. S. Ahn, S. Guha, and S. W. Cheong, *Nature (London)* **429**, 392 (2004).

²W. Eerenstein, N. D. Mathur, and J. F. Scott, *Nature (London)* **442**, 759 (2006).

³J. Wang, H. Zheng, Z. Ma, S. Prasertchoung, M. Wuttig, R. Droopad, J. Yu, K. Eisenbeiser, and R. Ramesh, *Appl. Phys. Lett.* **85**, 2574 (2004).

⁴L. W. Martin, Y. H. Chu, Q. Zhan, R. Ramesh, S. J. Han, S. X. Wang, M. Warusawithana, and D. G. Schlom, *Appl. Phys. Lett.* **91**, 172513 (2007).

⁵Z. V. Gabbasova, M. D. Kuz'min, A. K. Zvezdin, I. S. Dubenko, V. A. Murashov, D. N. Rakov, and I. B. Krynetsky, *Phys. Lett. A* **158**, 491 (1991).

⁶M. Polomska, W. Kaczmarek, and Z. Pajak, *Phys. Status Solidi* **23**, 567 (1974).

⁷Yu. E. Roginskaya, Yu. N. Venevtsev, S. A. Fedulov, and G. S. Zhdanov, *Sov. Phys. Crystallogr.* **8**, 490 (1964).

⁸K. Eisenbeiser, J. M. Finder, Z. Yu, J. Ramdani, J. A. Curless, J. A. Hallmark, R. Droopad, W. J. Ooms, L. Salem, S. Bradshaw, and C. D. Overgaard, *Appl. Phys. Lett.* **76**, 1324 (2007).

⁹Y. H. Chu, Q. Zhan, L. W. Martin, M. P. Cruz, P. L. Yang, F. Zavaliche, S. Y. Yang, J. X. Zhang, L. Q. Chen, D. G. Schlom, I. N. Lin, T. B. Wu, and R. Ramesh, *Adv. Mater. (Weinheim, Ger.)* **18**, 2307 (2006).

¹⁰A. V. Zalesski, A. A. Frolov, T. A. Khimich, and A. A. Bush, *Phys. Solid State* **45**, 141 (2003).

¹¹Y. H. Chu, M. P. Cruz, C. H. Yang, L. W. Martin, P. L. Yang, J. X. Zhang, K. Lee, P. Yu, L. Q. Chen, and R. Ramesh, *Adv. Mater. (Weinheim, Ger.)* **19**, 2662 (2007).

¹²V. L. Mathe, K. K. Patankar, M. B. Kothale, S. B. Kulkarni, P. B. Joshi, and S. A. Patil, *Pramana* **58**, 1105 (2002).

¹³H. Uchida, R. Ueno, H. Nakaki, H. Funakubo, and S. Koda, *Jpn. J. Appl. Phys., Part 1* **44**, L561 (2005).

¹⁴S. V. Kalinin, B. J. Rodriguez, S. Jesse, Y. H. Chu, T. Zhao, R. Ramesh, S. Choudhury, L. Q. Chen, E. A. Eliseev, and A. N. Morozovska, *Proc. Natl. Acad. Sci. U.S.A.* **104**, 5120204 (2007).